Lightning in Eastern North Pacific Tropical Cyclones: A Comparison to the North Atlantic

STEPHANIE N. STEVENSON AND KRISTEN L. CORBOSIERO

University at Albany, State University of New York, Albany, New York

SERGIO F. ABARCA

Environmental Modeling Center, I.M. Systems Group, and NOAA/NWS/NCEP, College Park, Maryland

(Manuscript received 5 August 2015, in final form 13 October 2015)

ABSTRACT

As global lightning detection has become more reliable, many studies have analyzed the characteristics of lightning in tropical cyclones (TCs); however, very few studies have examined flashes in eastern North Pacific (ENP) basin TCs. This study uses lightning detected by the World Wide Lightning Location Network (WWLLN) to explore the relationship between lightning and sea surface temperatures (SSTs), the diurnal cycle, the storm motion and vertical wind shear vectors, and the 24-h intensity change in ENP TCs during 2006–14. The results are compared to storms in the North Atlantic (NA).

Higher flash counts were found over warmer SSTs, with 28°–30°C SSTs experiencing the highest 6-hourly flash counts. Most TC lightning flashes occurred at night and during the early morning hours, with minimal activity after local noon. The ENP peak (0800 LST) was slightly earlier than the NA (0900–1100 LST). Despite similar storm motion directions and differing vertical wind shear directions in the two basins, shear dominated the overall azimuthal lightning distribution. Lightning was most often observed downshear left in the inner core (0–100 km) and downshear right in the outer rainbands (100–300 km). A caveat to these relationships were fast-moving ENP TCs with opposing shear and motion vectors, in which lightning peaked downmotion (upshear) instead. Finally, similar to previous studies, higher flash densities in the inner core (outer rainbands) were associated with nonintensifying (intensifying) TCs. This last result constitutes further evidence in the efforts to associate lightning activity to TC intensity forecasting.

1. Introduction

Lightning observations in tropical cyclones (TCs) over the open ocean were substantially limited prior to the development of global lightning detection networks in the early twenty-first century. Satellite instruments, such as the Optical Transient Detector (OTD) on board the *Microlab-1* satellite and the Lightning Imaging Sensor (LIS) on board the Tropical Rainfall Measuring Mission (TRMM) satellite, were the first observational platforms to provide a glimpse of total lightning (cloud-to-ground and intracloud) activity over the open oceans. The OTD instrument observed cloud-top lightning illumination with a 46%–69% detection efficiency and 20–40-km location accuracy during 1995–2000 (Boccippio et al. 2000). The LIS instrument, a follow-on to the OTD sensor, collected data during 1998–2015 with a detection efficiency of 62%–97% depending on the time of day (Boccippio et al. 2002). Cecil and Zipser (1999) analyzed the relationship between satellite-based lightning and TC intensity using the LIS. Since satellite observations only give a snapshot of the lightning activity over a short period of time, they found no clear association between lightning activity and TC intensification.

The National Lightning Detection Network (NLDN; Cummins and Murphy 2009) has been used to investigate the structure of lightning and its association to intensity change in North Atlantic basin TCs. Although the NLDN primarily captures lightning over land with a high detection efficiency (70%–90%; Cummins et al. 1998), the sensors are able to detect lightning occurring

Corresponding author address: Stephanie N. Stevenson, Department of Atmospheric and Environmental Sciences, University at Albany, State University of New York, 1400 Washington Ave., Albany, NY 12222.
E-mail: sstevenson@albany.edu

DOI: 10.1175/MWR-D-15-0276.1

within several hundred kilometers of the coast. Molinari et al. (1999) found that the radial distribution of lightning in TCs is characterized by a weak maximum in the eyewall region (or inner core, <100 km) and a strong maximum in the outer rainbands (210–290 km), with minimal lightning activity between the two regions. This radial distribution was found in satellite lightning data as well (Cecil and Zipser 1999). Corbosiero and Molinari (2002, 2003, hereafter CM03) showed that the azimuthal distribution of lightning in TCs is dominated by the direction of the deep-layer vertical wind shear rather than the storm motion. Lightning was found to occur primarily downshear left in the inner core and downshear right in the outer rainbands. From their examination of nine North Atlantic TCs, Molinari et al. (1999) hypothesized that outbreaks of lightning in the inner core of a weakening, steady, or slowly deepening TC may indicate rapid intensification, whereas outbreaks in TCs deepening for some time may signal an end to intensification.

Global lightning detection networks, like the World Wide Lightning Location Network (WWLLN) and Vaisala's Global Lightning Dataset (GLD360; Holle and Murphy 2015), have expanded the range of TC lightning detection, since they are capable of detecting lightning over the open oceans. The WWLLN has recorded lightning data for five more years than the GLD360; thus, most of the recent TC lightning studies have utilized the WWLLN. The radial and azimuthal distributions discussed above have been supported by global WWLLN data (Pan et al. 2010; Abarca et al. 2011). Since the WWLLN provides continuous lightning detection away from landmasses, studies have also analyzed the intensity change signaled by the lightning activity, with varying results. Price et al. (2009) studied major hurricanes around the globe and found increased lightning activity one day prior to peak intensity. Pan et al. (2010, 2014) and Zhang et al. (2015) also found a peak in lightning activity prior to peak intensity in northwest Pacific typhoons. However, Thomas et al. (2010) and DeMaria et al. (2012) noted the exact opposite—weakening following an inner core lightning outbreak—in North Atlantic and eastern North Pacific TCs. Additionally, DeMaria et al. (2012) noted intensification 24 h after increased lightning activity in the outer rainbands, a relationship that was stronger in the eastern North Pacific basin.

Although the DeMaria et al. (2012) study examined the relationship of lightning activity to TC intensity change in eastern North Pacific TCs, only one other study is known to focus on the characteristics of TC lightning in this basin. Leary and Ritchie (2009) analyzed lightning flash rates from Vaisala's Long-Range Lightning Detection Network (Cummins et al. 1999) in developing and nondeveloping tropical cloud clusters. They found that the National Hurricane Center (NHC) designated developers had, on average, 142 more flashes per 6-h period than the cloud clusters that did not develop into TCs. While both of these studies have promising results, a comprehensive analysis of lightning in TCs in the eastern North Pacific has not been performed.

Although most eastern North Pacific TCs never make landfall, many do and generate disasters over western Mexico (Farfán et al. 2013). Eastern North Pacific TCs also impact shipping routes, cause terrain-enhanced heavy rainfall over Mexico (Camargo et al. 2008), and contribute to the summer precipitation in the southwestern United States (Corbosiero et al. 2009). The eastern North Pacific basin is the most active TC formation region on Earth in terms of genesis events per unit area per unit time (Molinari et al. 2000) and second most active basin globally (Gray 1968); thus, the number of TCs occurring in this basin can aid in the general understanding of lightning activity in TCs. Furthermore, since few aircraft reconnaissance flights occur in the eastern North Pacific, understanding the characteristics of lightning in TCs, and its potential signals for TC intensity change, could help to improve intensity forecasts. The upcoming launch of the Geostationary Operational Environmental Satellite R-series (GOES-R) and its Geostationary Lightning Mapper (GLM; Goodman et al. 2013) instrument in 2016 provides incentive for understanding TC lightning activity so the GOES-R GLM data can be used to their full potential. This study aims to provide such understanding by analyzing the lightning characteristics of eastern North Pacific TCs using a ground-based lightning network.

Section 2 describes the data and methods used in this study. The lightning patterns with respect to sea surface temperature, the diurnal cycle, radius and azimuth, and TC intensity change are discussed in sections 3a, 3b, 3c, and 3d, respectively. A summary of the results is presented in section 4.

2. Data and methods

This study analyzes TCs in the eastern North Pacific (ENP) and North Atlantic (NA) basins that occurred during 2006–14. The position (Fig. 1) and intensity for all TCs were obtained from the NHC best track dataset, a subjectively smoothed dataset created using all the data available poststorm (i.e., satellite and/or aircraft reconnaissance) at the 6-hourly synoptic times (0000, 0600, 1200, and 1800 UTC; Landsea and Franklin 2013). The 6-hourly positions were used to compute storm motion

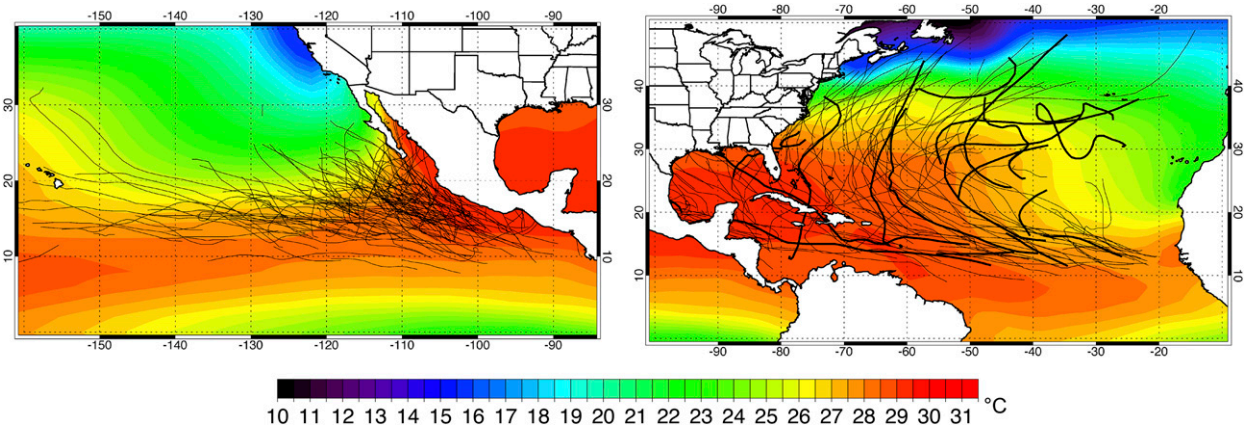

FIG. 1. NHC best track locations for TCs in the (left) eastern North Pacific and (right) North Atlantic during 2006–14. Thicker tracks in the North Atlantic correspond to TCs in 2012 (see text). Tracks are only present for storms with tropical depression or greater strength. The climatological 1981–2010 mean September SSTs (shaded; °C) are from the NOAA Extended Reconstructed SST V3b.

vectors. In total, 155 (135) TCs occurred in the ENP (NA) during these years. For simplicity, analyses will be performed using individual time periods (ITPs; Table 1), or 6-h time periods that align with the best track dataset. This results in a robust sample of 3768 (3870) total ITPs to study in the ENP (NA).

a. Lightning

The WWLLN (operated by the University of Washington; http://wwlln.net) is utilized for locating lightning flashes. The WWLLN is a global, ground-based network that detects lightning through a time-of-arrival technique. Lightning emits very low-frequency radio waves (''sferics'') that travel through the Earth–ionosphere waveguide. This signal is received by ground sensors located around the globe; the network requires at least five sensors to accurately locate lightning, with each sensor capable of detecting lightning several thousands of kilometers away. The reliance of the WWLLN on the Earth–ionosphere waveguide results in some detection efficiency differences depending on the time of day since the ionization density changes between day and night (Watt 1967); at nighttime, sferics are able to propagate farther distances due to lower attenuation. Rodger et al. (2006) found the detection range of WWLLN's Darwin, Australia, station increased from ~8000 km at local noon to ~12 000 km at local midnight.

Abarca et al. (2010) estimated that the overall lightning detection efficiency was around 10% for cloud-to-ground flashes over the continental United States in 2008–09 (although the WWLLN detects intracloud flashes as well, the detection efficiency is much lower for those weaker flashes). Rudlosky and Shea (2013) showed that the WWLLN detection efficiency was greater over the oceans than over land; the WWLLN detects stronger flashes more efficiently (Abarca et al. 2010) and stronger flashes tend to occur in oceanic convection (Hutchins et al. 2013). For the two basins included in this study, Rudlosky and Shea (2013) suggested the detection efficiencies range from 25% to 50% over the ENP and from 15% to 25% over the NA (see their Fig. 1). Despite the rather low detection efficiencies, Abarca et al. (2011) found that the spatial distribution of lightning flashes in TCs correlates quite well to the higher detection efficiency NLDN.

The lightning flashes were transformed from a geographical coordinate system (i.e., latitude and longitude) into a cylindrical coordinate system (i.e., radius and azimuth) centered on the TC. The NHC best track positions were linearly interpolated to 1-min intervals to calculate the radius and azimuth. Although the best track often misses the erratic behavior of TC movement (Landsea and Franklin 2013), Stevenson et al. (2014) found the distribution of lightning flashes to be very similar using location datasets with finer time resolution (e.g., flight reconnaissance). Only flashes located within 300 km of the TC center were of interest for this study, and only ITPs with at least one lightning flash were analyzed.

TABLE 1. The total number of 6-hourly individual time periods investigated in this study, binned according to NHC best track intensity, for the eastern North Pacific and North Atlantic TCs during 2006–14.

	Eastern North Pacific	North Atlantic
TDTS	2988	3039
H1H2	565	668
H3H5	215	163
Total	3768	3870

The number of sensors in the WWLLN has continued to grow over time since the network was first established in the early 2000s (Lay et al. 2004). There were 25 sensors in operation in 2006 (Rodger et al. 2006) and over 70 sensors currently (Hutchins et al. 2013). Figure 2 shows the number of lightning flashes per ITP detected within a 300-km radius of the TC center (solid lines), as well as the total number of lightning flashes detected in the basin during respective NHC-defined TC seasons (dashed lines; basin bounded by latitude and longitude ranges shown in Fig. 1), for both the ENP (black) and NA (gray) during each year of this study. A steady increase in the amount of lightning flashes detected is observed, as expected with the growing number of sensors in the network. It is worth noting that the minimum in the 2012 NA 0–300-km flash count could be a reflection of the storms occurring farther north and east, over cooler sea surface temperatures (see bold tracks in Fig. 1) or in a region with decreased detection efficiency [see Fig. 1a in Rudlosky and Shea (2013) for the spatial distribution of WWLLN detection efficiency in 2012]. Given the increased detection of lightning flashes over the nine years in this study, the authors chose to normalize any results using WWLLN flash count and flash density to reduce weighting the results toward the latter years. Since different normalization techniques were applied for different analyses, a description of the normalization method will be given in the text prior to the introduction of normalized figures.

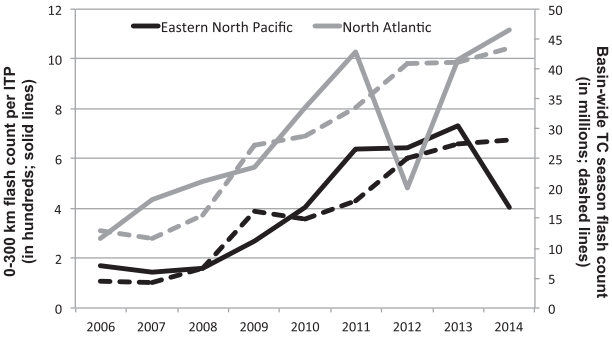

FIG. 2. WWLLN flash counts within 300 km of the TC center normalized by the number of ITPs per year (in hundreds; solid lines) and basin flash counts for each TC season (in millions; dashed lines) in the eastern North Pacific (black) and North Atlantic (gray).

b. *Environmental measurements*

The relationship of lightning flashes to environmental parameters, such as sea surface temperature (SST) and vertical wind shear, from the Statistical Hurricane Intensity Prediction Scheme (SHIPS; DeMaria and Kaplan 1994) were examined. SHIPS evaluates a Reynolds SST value (Reynolds and Marsico 1993) at the storm center from weekly 1° resolution analyses. The vertical wind shear is calculated using the National Centers for Environmental Prediction (NCEP) Global Forecast System (GFS) analyses over a deep layer (850–200 hPa) and is azimuthally averaged between 200- and 800-km radii to remove the symmetric component of the TC vortex.

3. Results and discussion

a. *Relationship to SST*

The relationship between lightning flash count and SST has not been studied extensively, especially in TCs, most likely due to lack of continuous lightning observations over the ocean prior to the last decade or so. Climatological lightning density from the WWLLN and LIS/OTD [see Fig. 2 in Virts et al. (2013)], and the GLD360 [see Fig. 1 in Holle and Murphy (2015)], suggest that more flashes occur over warmer SSTs; the warm Gulf Stream off the eastern U.S. coastline and the warmest waters just offshore of western Mexico are evident in both lightning climatologies. Similar to Virts et al. (2015)'s finding of a lightning maximum over the Gulf Stream, which is characterized by a strong SST gradient, our study of TC lightning shows a maximum in this area as well (Fig. 3).

Figure 4 is a scatterplot of the flash count within 300 km of a TC versus Reynolds SST for each ITP. Both the ENP and NA show similar patterns, with increased SSTs supporting larger TC flash counts. Below 26°C (25°C) in the ENP (NA), values struggle to exceed 1000 flashes in a 6-h time period. This is the approximate threshold (26°C) in one of Gray (1968)'s necessary, but not sufficient, thermodynamic constraints to support deep convection for tropical cyclogenesis. The ''sweet spot'' for high lightning flash counts falls between 28° and 30°C for both basins.

A study by Waliser and Graham (1993) found that the intensity of oceanic convection increases sharply from 26.5° to 29°C, reaches a maximum at 29.5°C, and declines at higher SSTs, similar to the pattern of lightning flash counts found in our study. More water is present in the lower troposphere in a higher SST environment, and the combination of these two factors increases the moist static energy and convective available potential energy (CAPE) to allow parcels to ascend to the upper troposphere (Trenberth 2005). Fu et al. (1994) show that SSTs $\geq$ 28°C always have positive CAPE, where SSTs $<$ 27°C generally have a convectively stable atmosphere in the

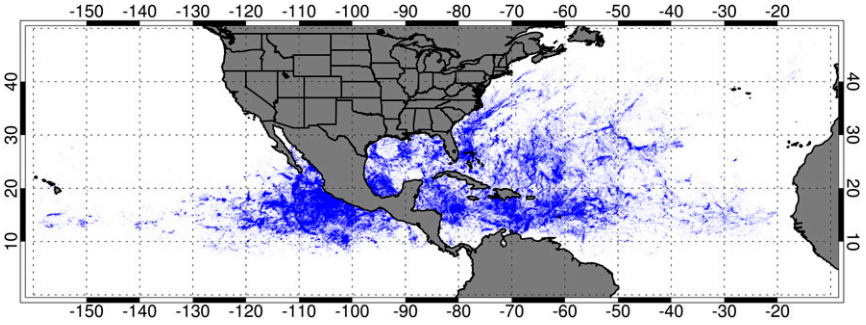

FIG. 3. WWLLN oceanic flash locations (blue dots) within 300 km of eastern North Pacific and North Atlantic TCs during 2006–14.

absence of strong surface wind convergence. These convective relationships to SSTs, along with Romps et al. (2014)'s finding that lightning flash rate over land is proportional to the product of precipitation and CAPE, suggest that SSTs in the range of 28°–30°C provide an environment that supports stronger convection and more lightning activity. Although the reason for reduced convective activity above 29.5°C is not fully understood, Lau et al. (1997) propose one theory that the lack of convection is influenced by large-scale subsidence forced by nearby convection. They suggest the subsidence adiabatically warms and dries the atmosphere above the boundary layer, creating a temperature inversion, and promotes more insolation and higher SSTs under clear skies. Given the low sample size above 30°C in our study, it is unclear if the reduction of lightning flash counts at higher SSTs is a robust result.

The TC tracks in the ENP traverse a smaller range of SSTs than TCs in the NA, as shown in Fig. 5. Most of the ITPs in NA TCs occur in a range from 22° to 31°C, while the ENP range is smaller, from 24° to 31°C. The wider range in the NA can be attributed to recurving TCs entering the midlatitudes, while TCs in the ENP rarely reach latitudes larger than 25°–30°N (Fig. 1). Also of note from Fig. 5 is the positive trend in SST and storm intensity, suggesting that major hurricanes occur over warmer SSTs than tropical depressions or tropical storms, as expected.

b. *Diurnal cycle*

The diurnal cycle of lightning flash counts within 300 km of TCs varies between the ENP and NA (Fig. 6). The diurnal cycle was normalized by 1) dividing the flash count in each LST bin for each year by the number of TCs occurring in that bin, 2) normalizing the hourly bins by the maximum for each year, and 3) summing each hourly bin over all the years and normalizing by the maximum again. The final normalized value from 0.0 to 1.0 is plotted in Fig. 6. In the NA, there is an early morning maximum, occurring at 0100 LST, with a weaker, secondary maximum in the late morning between 0900 and 1100 LST. The ENP has elevated lightning activity from 1700 to 0900 LST, with a peak at 0800 LST, and suppressed activity near local noon. The

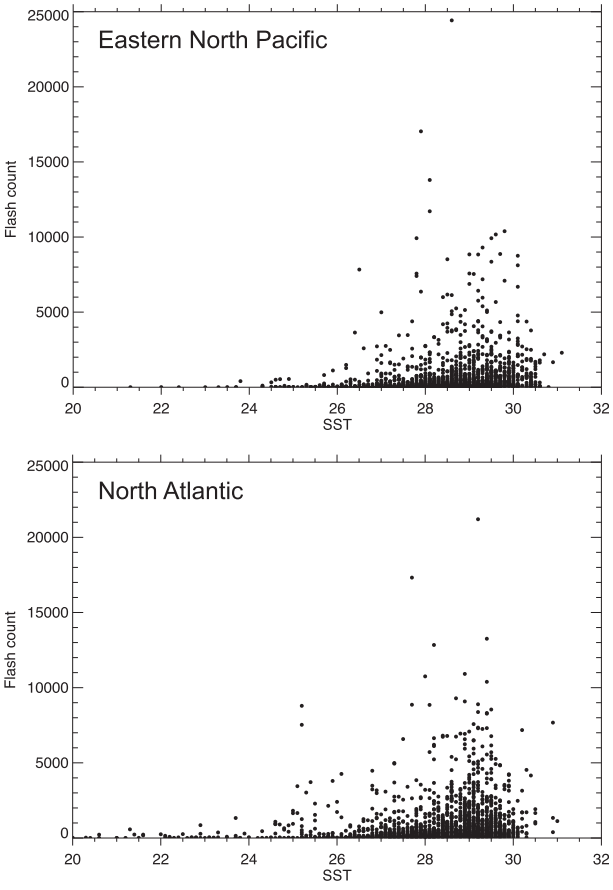

FIG. 4. The 6-hourly WWLLN flash counts within 300 km of (top) eastern North Pacific and (bottom) North Atlantic TCs as a function of Reynolds SST.

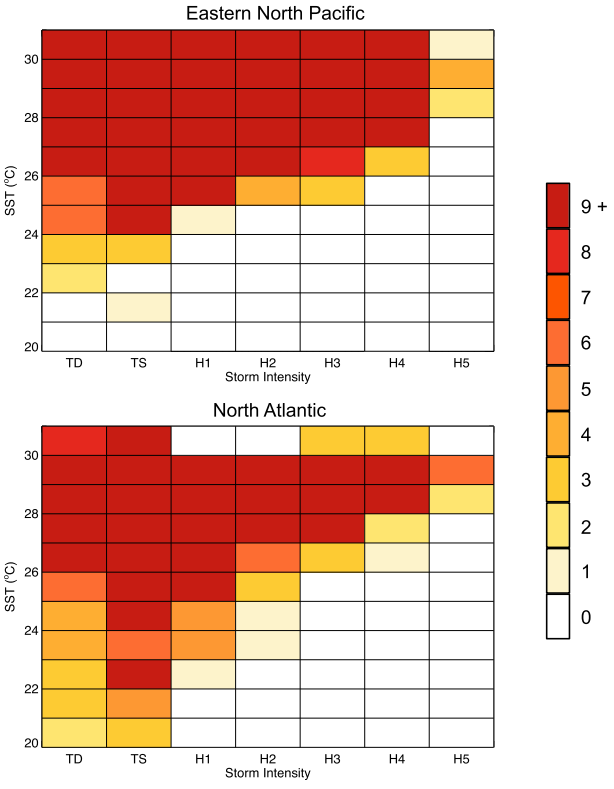

FIG. 5. The number of 6-hourly individual time periods (colors) corresponding to a given Reynolds SST and TC intensity for the (top) eastern North Pacific and (bottom) North Atlantic.

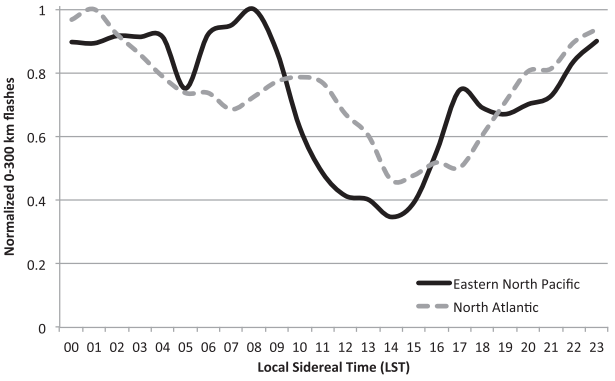

FIG. 6. The normalized number of lightning flashes within 300 km of TCs as a function of the local sidereal time (LST) for the eastern North Pacific (solid black) and North Atlantic (dashed gray). See text for a description of the normalization.

more active part of the diurnal cycle in both basins generally fell during the overnight hours, which is expected in convection over the oceans (Gao and Li 2008).

Previous studies on oceanic convection have found varying hours of peak activity, but generally agree that the diurnal cycle over the ocean has a smaller amplitude than over land (Gray and Jacobson 1977). Although there is no direct relationship between lightning and cloud-top temperatures, rainfall distributions, or rain rates, the diurnal variability of these other convective indicators can provide insight into the diurnal cycle of oceanic convection. Janowiak et al. (1994) showed that the coldest cloud-top temperatures over the tropical oceans occurred between 0300 and 0600 LST. Kossin (2002)'s analysis of GOES infrared imagery revealed a significant semidiurnal cycle in the inner core, especially for stronger TCs. Our results are not inconsistent with his findings (not shown), but the noise present in the inner core lightning field make it difficult to determine the significance of any semidiurnal signal. Total rainfall, measured by TRMM, found an early morning maximum near sunrise (0600 LST), similar to the coldest cloud tops (Nesbitt and Zipser 2003). Restricting the TRMM data to a 500-km radius around TCs, Bowman and Fowler (2015) found that mean rain rates also peak at 0600 LST and reach a minimum in the afternoon around 1800 LST; this diurnal cycle varies slightly between the ENP and NA basins. A previous study using WWLLN data noted a morning peak over the ocean (0800 LST) and a minimum in the late afternoon (Lay et al. 2007). This peak aligns well with our observations of ENP TCs; however, activity was found to increase again in the late afternoon rather than be minimized (Fig. 6). Gao and Li (2008) mention that a secondary maximum of oceanic convection in the afternoon may be linked to daytime SST increases.

The diurnal cycle of WWLLN lightning flashes over the warm Gulf Stream in the NA was analyzed by Virts et al. (2015). Although they found a broad nighttime maximum, two peaks were noted within the broad maximum: one a few hours after midnight, and another in the morning hours between 0800 and 1100 LST. Despite most of the lightning analyzed in our study occurring in regions without a sharp SST gradient like the one present in the Gulf Stream, we found NA TCs to exhibit a similar diurnal cycle with peak activity occurring during the same times. Virts et al. (2015) partially attributed the nocturnal maximum to a wind shift from a sea breeze during the day to a land-breeze configuration at night. Kucienska et al. (2012) found a similar diurnal contrast between the land and ocean lightning activity in the ENP due to the land- and sea-breeze circulations, with the maximum lightning activity over the ocean in the morning hours.

Dunion et al. (2014) showed evidence of a diurnal cycle in mature hurricanes in satellite infrared brightness temperatures that is characterized by cold cloud tops, potentially associated with deep convection, propagating radially outward. The cooler cloud tops begin forming in the storm's inner core near local sunset and move outward to a radius of 300 km by local noon.

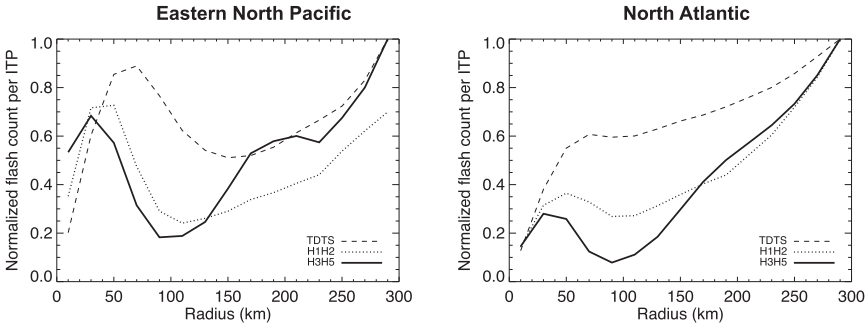

FIG. 7. Normalized lightning flash counts per ITP calculated in 20-km radial bins in the (left) eastern North Pacific and (right) North Atlantic. See text for a description of the normalization. The three radial distributions represent varying TC strength [TDTS (dashed line), H1H2 (dotted line), and H3H5 (solid line)].

These "pulses" extend beyond 300 km between local noon and sunset, which coincides somewhat with the minimum lightning activity seen in Fig. 6. Although it is not shown in this paper, the authors have found a radially propagating diurnal cycle in the lightning field, similar to Dunion et al. (2014), in select ENP and NA TCs. More research is necessary to delineate the causes of the observed diurnal lightning patterns in TCs and to investigate if these signals are robust given Abarca et al. (2010)'s finding that the WWLLN did not capture the diurnal cycle over the continental United States in a comparison to the NLDN. Like the WWLLN, other global datasets that capture oceanic lightning, such as the LIS and OTD (Cecil et al. 2014), have a reduced detection efficiency around local noon, which further complicates quantifying the diurnal cycle over the open ocean.

c. *Lightning distribution in TCs*

1) RADIAL DISTRIBUTION

The typical radial distribution of lightning flashes in TCs includes a weak maximum in the eyewall and a strong maximum in the outer rainbands (Molinari et al. 1999). The radial distributions of normalized lightning flash counts per ITP for the ENP and NA are shown in Fig. 7. The radial plots were constructed by normalizing the radial distribution for each ITP by the maximum, summing these values in each radial bin for all ITPs, and normalizing again by the maximum. In the ENP, tropical depressions and tropical storms (collectively TDTS) have peaks in flash count around 70 and 290 km, corresponding well with the eyewall and outer rainband maxima described by Molinari et al. (1999). The eyewall maximum moves radially inward with increasing storm strength [50 km for weak hurricanes (H1H2) and 30 km for major hurricanes (H3H5)], likely in association with eyewall contraction as storms intensify (Shapiro and Willoughby 1982; Willoughby 1990), but the outer rainband maximum remains around 290 km. A similar pattern is noted in the NA, except somewhat more subtle in the TDTS strength storms. The size of weaker TCs (i.e., TDTS) in the NA varies more than those in the ENP (Knaff et al. 2014); thus, the distribution of lightning flashes in the eyewall region is more likely to vary in radial location.

For the remainder of the paper, lightning flashes will be segregated into two radial regions: the inner core (0–100 km; encompassing the eyewall region) and the outer rainbands (100–300 km). The 100-km separation between the inner core and the rest of the TC is common in studies analyzing lightning in TCs (Corbosiero and Molinari 2002; CM03; Abarca et al. 2011; DeMaria et al. 2012; Pan et al. 2014) and is supported by this study. The number of ITPs with at least one lightning flash in each radial region for the varying storm intensities is shown in Table 2 (note: the sample size decreases for increasing storm intensity).

2) AZIMUTHAL DISTRIBUTION

Corbosiero and Molinari (2002) and CM03 showed the dependence of asymmetric convection (i.e.,

TABLE 2. The number of 6-hourly individual time periods in each TC intensity category and radial region where at least one lightning strike occurred for the eastern North Pacific and North Atlantic.

	Eastern North Pacific		North Atlantic	
	Inner core	Outer bands	Inner core	Outer bands
TDTS	1063	1354	1182	1590
H1H2	226	280	342	483
H3H5	133	138	123	150
Total	1462	1772	1647	2223

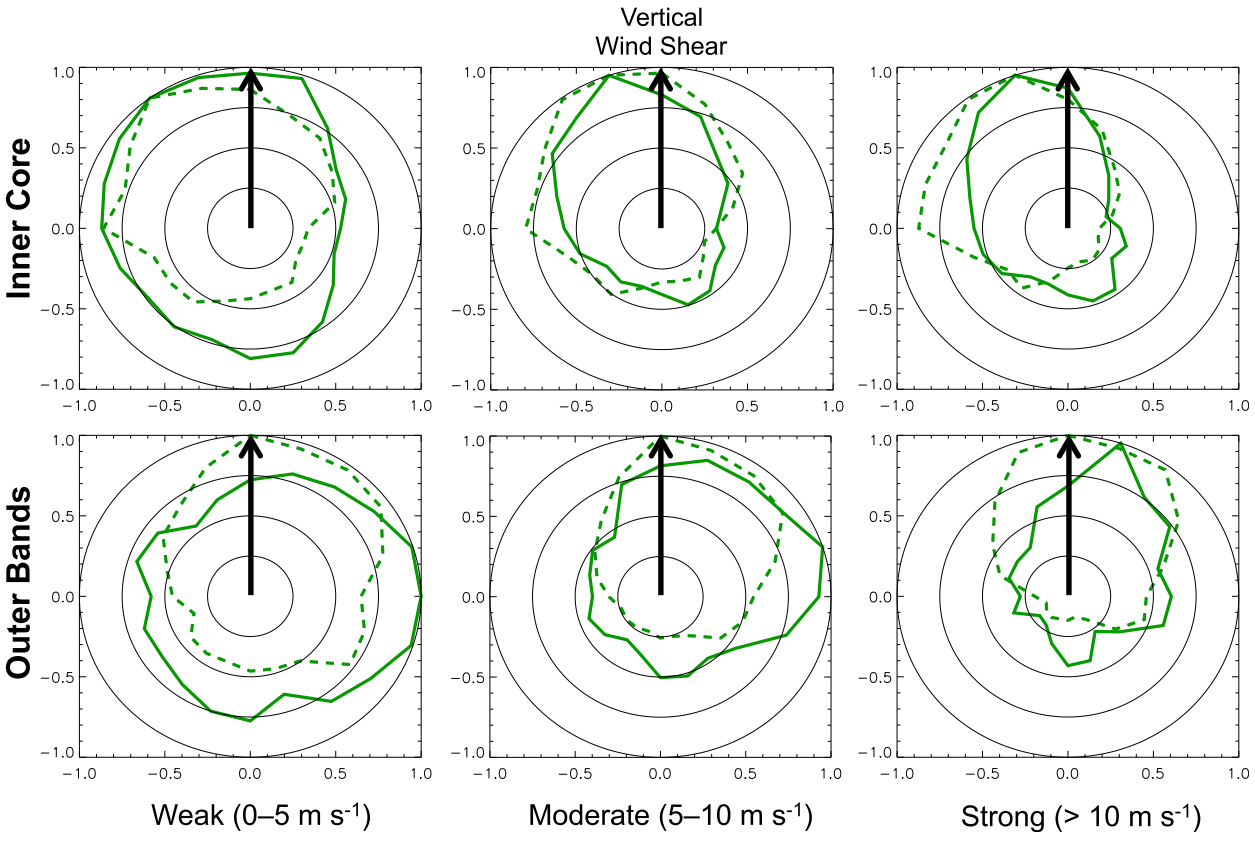

FIG. 8. Icosagons indicating the most common locations of lightning flashes in the (top) inner core and (bottom) outer rainbands with respect to the shear vector (black arrow) for eastern North Pacific (solid) and North Atlantic (dashed) TCs. The icosagons are displayed for various shear values: (left) weak (0–5 m s^{-1}), (middle) moderate (5–10 m s^{-1}), and (right) strong (>10 m s^{-1}).

lightning) on storm motion and vertical wind shear in NA basin TCs. A similar analysis was performed on the ENP and NA TCs in this study with icosagons to analyze the location of the maximum lightning activity relative to the shear and motion vectors. The icosagons are created in a manner similar to Abarca et al. (2011), as follows: 1) lightning flashes are summed in 20 azimuthal bins (18° spacing) for each individual ITP; 2) the flash counts are normalized by the maximum value, giving all 20 azimuthal bins a value from 0.0 to 1.0; 3) all the normalized values for individual ITPs are summed together; and 4) these sums are normalized again by the maximum value. The resulting normalized values from 0.0 to 1.0 are plotted in the icosagons shown in Figs. 8 and 9. Table 3 shows the number of ITPs that were included in each icosagon.

The shear icosagons between the two basins are nearly identical (Fig. 8). For weak (0–5 m s^{-1}), moderate (5–10 m s^{-1}), and strong (>10 m s^{-1}) vertical wind shear, both the ENP and NA had lightning peaks in the downshear left quadrant in the inner core and in the downshear right quadrant in the outer rainbands. These azimuthal preferences narrow and become more defined with increasing shear magnitude. Downshear left is the expected location of convection in the inner core given TC vortex dynamics. In a sheared environment, the vertical wind shear acts to tilt the TC vortex downshear. This horizontally displaces the TC's positive potential vorticity anomaly at mid- to upper levels from the positive, low-level potential vorticity anomaly, and through vertical projections of these anomalies onto one another, the tilted vortex begins to precess cyclonically (Jones 1995). The optimal vortex tilt configuration is downshear left, where the differential advection from the precession process and the shear balance each other. The secondary circulation becomes stronger in response to a tilted vortex, thus increasing the vertical motions (and convection) downtilt in an effort to realign the vortex into an upright position (Reasor et al. 2004). The preference for downshear right in the outer rainbands can be explained by adiabatic processes. In a sheared environment, ascent downshear creates a cold potential temperature anomaly via vertical advection, and descent upshear creates a warm potential temperature

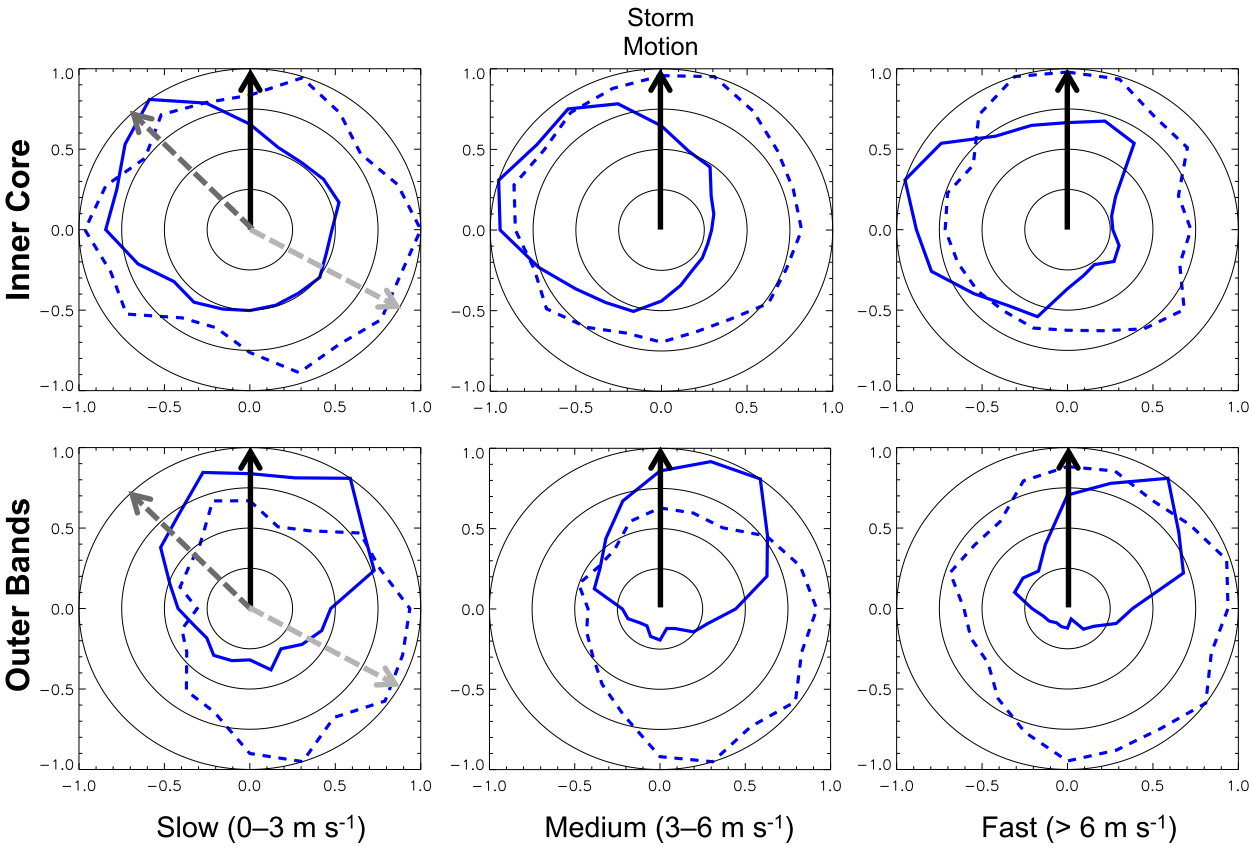

FIG. 9. Icosagons indicating the most common locations of lightning flashes in the (top) inner core and (bottom) outer rainbands with respect to the motion vector (black arrow) for the eastern North Pacific (solid) and North Atlantic (dashed). The icosagons are displayed for various motion values: (left) slow (0–3 m s^{-1}), (middle) medium (3–6 m s^{-1}), and (right) fast (>6 m s^{-1}). The dashed arrows in the slow motion icosagons indicate a representative shear vector for the eastern North Pacific (dark gray) and North Atlantic (light gray).

anomaly (Jones 1995). Jones (1995)'s numerical simulations show that the outer rainband region is more strongly tilted than the inner core region (see her Fig. 6). As parcels are advected cyclonically around the TC vortex in the outer regions, parcels must rise to the right of the shear vector to conserve their potential temperature.

Despite similarities in the shear icosagons, the lightning distributions with respect to motion are noticeably different between the two basins (Fig. 9). In the inner core of ENP TCs, lightning is favored left and front of motion at all speeds (slow: 0–3 m s^{-1}, medium: 3–6 m s^{-1}, and fast: >6 m s^{-1}). In the inner core of NA TCs, lightning is rather azimuthally uniform, with a slight preference front of motion at medium and fast speeds. Differences between the ENP and NA are also observed in the outer rainband lightning: although both basins have peak lightning right of motion, the ENP peaks in the right-front quadrant, while the NA peaks in the right-rear quadrant. CM03 also found a right-front quadrant preference in the inner 100 km and a right of motion preference in the outer rainbands of NA TCs; however, our results from a much larger sample size found the outer rainband maximum to occur in the right-rear quadrant rather than the right-front quadrant. Convection is favored downmotion since frictional convergence is usually maximized in that quadrant (Shapiro 1983); however, Frank (1977) showed that rainfall, which includes both stratiform and convective components, was highest in the right-rear quadrant of northwest Pacific TCs, similar to the observation of peak lightning in NA TCs in this study.

The relationship between the shear and motion vectors differs between the two basins (Fig. 10; note: the angle is measured counterclockwise from the shear vector to the motion vector). Angles between the shear and motion peak from 45° to 165° in the NA, similar to the peak angle difference found by CM03. Vector differences are much larger in the ENP, peaking from 270° to 345°. Both basins have storm motions that are predominately westward to northwestward; however, the NA has westerly deep-layer vertical

TABLE 3. The number of 6-hourly individual time periods included in the motion and shear icosagons in Figs. 8 and 9 for the eastern North Pacific and North Atlantic.

	Eastern North Pacific	North Atlantic
Motion		
Slow (0–3 m s^{-1})	519	388
Medium (3–6 m s^{-1})	1117	930
Fast (>6 m s^{-1})	348	922
Shear		
Weak (0–5 m s^{-1})	844	545
Moderate (5–10 m s^{-1})	889	1021
Strong (>10 m s^{-1})	251	674

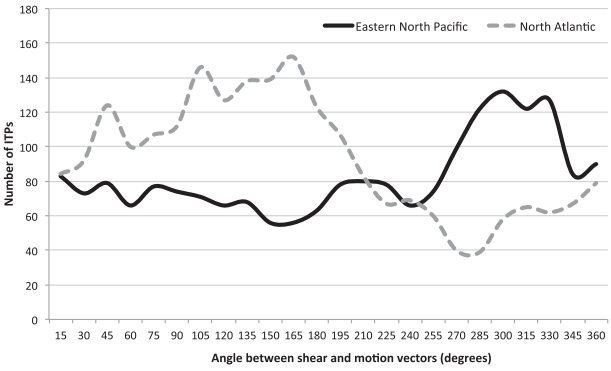

FIG. 10. Histogram of the number of 6-hourly individual time periods (ITPs) corresponding to various angles between the shear and motion vectors for eastern North Pacific (solid black) and North Atlantic (dashed gray) TCs. The angle is measured counterclockwise from the shear vector to the motion vector.

wind shear, while the ENP has easterly shear (Chen et al. 2006).

An interesting and unique difference emerged when convective asymmetries in the lightning field were compared for ITPs where the shear and motion vectors were either aligned or opposed to one another (Fig. 11). When the shear and motion were aligned, lightning in both basins occurred downshear left (front and left of motion) in the inner core and downshear right (front and right of motion) in the outer rainbands. The same relationships were also true for ITPs with opposing shear and motion vectors in the NA. However, motion appears to modulate the lightning asymmetries when the shear and motion oppose each other in the ENP basin, with the maximum in lightning flashes occurring downmotion (upshear) rather than downshear. Hints of this relationship appear in the shear icosagons in Fig. 8, where a stronger lightning signal appears upshear in the ENP, especially for weak shear cases. This downmotion pattern is predominately driven by storms with a faster translation speed; higher shear magnitude resulted in convection in the expected downshear quadrants (not shown). Chen et al. (2006) and Thomsen et al. (2015) suggest that faster translation speeds are more likely to induce motion asymmetries in the convective distribution. Our observed lightning results suggest this may be true for the ENP, but does not appear to be the case for the NA. The differences found in the ENP faster translation ITPs with opposing shear and motion vectors are not yet fully understood; the authors are presently working on diagnosing this signal and will report the findings in a future study.

The results of this study support the findings of CM03 that vertical wind shear dominates over the distribution of convection over storm motion in the NA. Despite directional differences between the shear and motion vectors in the basins, shear appears to play a more important role in the ENP as well, especially for stronger shear magnitudes. The distribution of lightning flashes that appear in the motion icosagons are largely an artifact of the relationship between the shear and storm motion vectors. As noted previously, the shear vector is approximately 270°–345° right of the motion vector in the ENP and 45°–165° right of motion in the NA. Placing a representative shear vector for each basin on the motion icosagons in Fig. 9 (dashed gray arrows) solidifies that lightning activity is downshear left in the inner core and downshear right in the outer rainbands.

d. *Relationship to intensity changes*

Several recent studies have found an association between increased lightning activity and intensity changes in TCs (Price et al. 2009; Thomas et al. 2010; Pan et al. 2010, 2014; DeMaria et al. 2012; Stevenson et al. 2014), as discussed in section 1. Figures 12 and 13 show the normalized average flash density in the inner core and outer rainbands, respectively, of intensifying and nonintensifying TCs in the subsequent 24 h in the ENP and NA. These plots were normalized to reduce the impact of the increase in flash density due to network improvement (Fig. 2) on the results. For each year, an average flash density was computed for intensifying and nonintensifying cases, and both were normalized by the maximum of the two subsets. The years were then summed together for each subset and normalized by the maximum again. Statistical significance of the difference between normalized average flash densities was tested at the 95% confidence interval using a 1000-iteration bootstrap resampling with replacement.

Higher inner core flash densities tended to occur in nonintensifying TCs in both basins (Fig. 12). For the weakest storms (TDTS), the normalized flash density

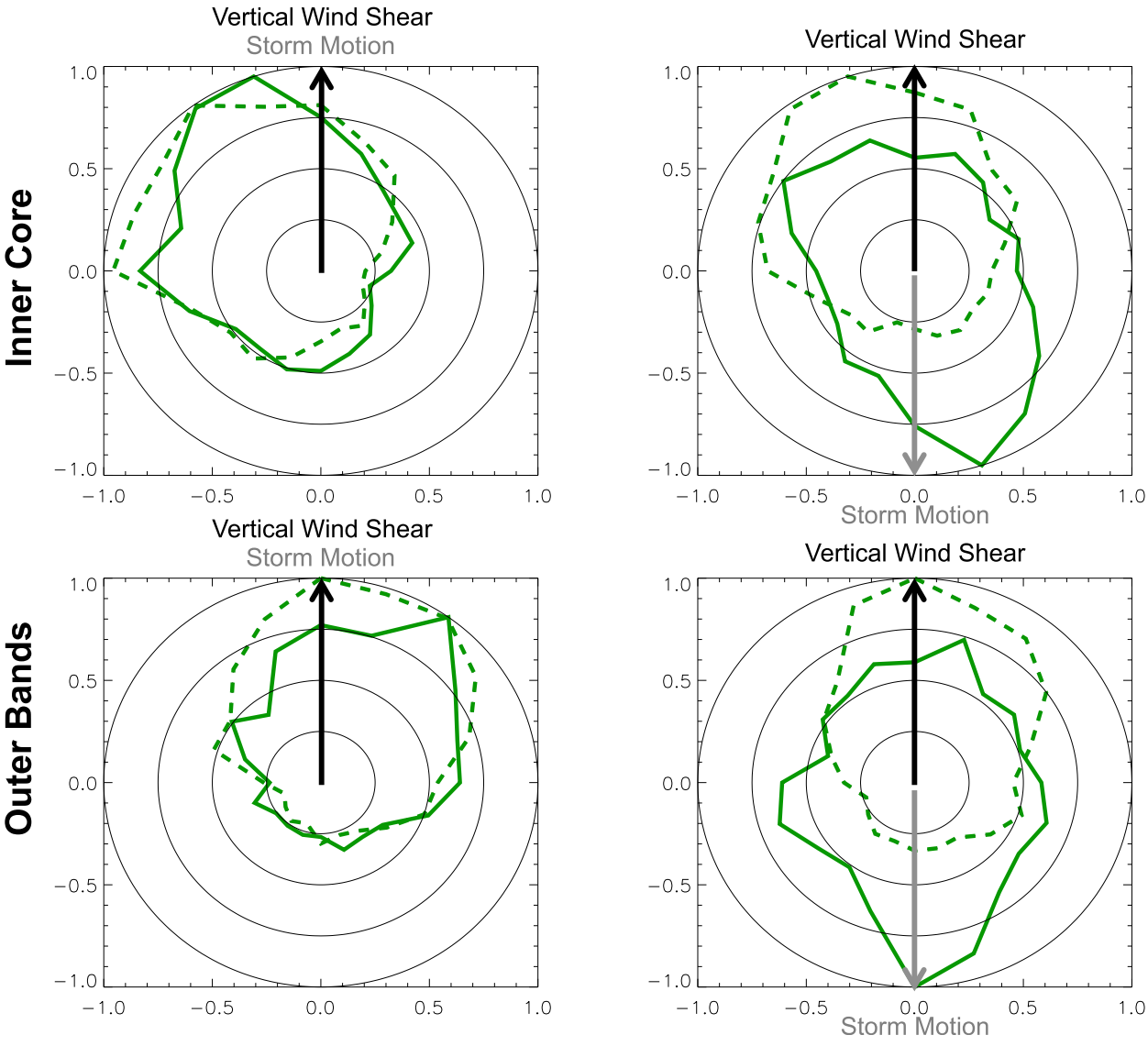

FIG. 11. Icosagons indicating the most common locations of lightning flashes in the (top) inner core and (bottom) outer rainbands with respect to the shear (black arrow) and motion (gray arrow) vector for the eastern North Pacific (solid) and North Atlantic (dashed). (left) ITPs where the shear and motion vector are aligned (>337.5° and <22.5°), and (right) ITPs where the shear and motion vector are opposed (157.5°–202.5°). All motion speeds and shear magnitudes are included.

in nonintensifying TCs was larger in both the ENP and NA, though only the ENP signal was significant. Weak hurricanes (H1H2) in both basins had statistically significantly higher flash densities in nonintensifying TCs as well. Major hurricanes (H3H5) show a differing relationship between the ENP and NA, but neither result is significant. As Abarca et al. (2010) suggested, flash density in the inner core of weaker TCs seems to have more potential in distinguishing intensifying versus nonintensifying TCs. It is worth noting that the radial limit of the inner core at 100 km may not be encompassing the entire inner core region for TCs with a larger radius of maximum wind (RMW), especially for weaker storms (TDTS).

The weakening response of TCs to higher lightning flash densities in the inner core found in our study matches the results of DeMaria et al. (2012), who used adjusted WWLLN data to analyze 2005–10 ENP and NA TCs. In contrast, Stevenson et al. (2014) showed a NA TC case with an inner core lightning burst prior to a period of rapid intensification, suggesting that there is more to the story than simply an increased number of lightning flashes. We hypothesize that higher flash densities in the inner core can signal both

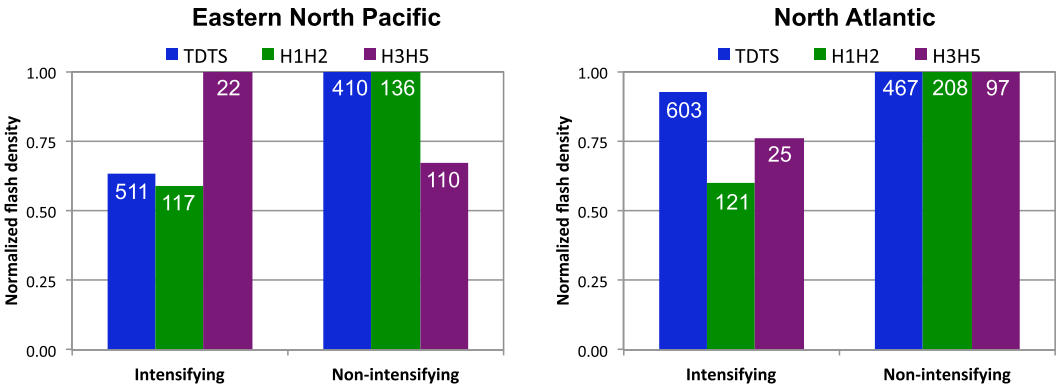

FIG. 12. The normalized flash density in the inner core (0–100 km) for intensifying and nonintensifying TCs (based on 24-h intensity change) in the (left) eastern North Pacific and (right) North Atlantic. See text for a description of the normalization. The colors represent varying TC strengths [TDTS (blue), H1H2 (green), and H3H5 (purple)]. The number of ITPs averaged in each bar is noted at the top of the bars.

intensification and weakening, dependent on the location of the lightning relative to the RMW (i.e., whether it is located inside or outside the inertially stable core). Rogers et al. (2013) showed convective bursts located inside the RMW were preferred in intensifying TCs, while steady-state TCs tended to have convective bursts outside the RMW. Stronger convection (and more lightning) inside the RMW would radially confine the diabatic heating and further warm the TC core (Vigh and Schubert 2009), while convection outside the RMW may slow intensification or even cause weakening. Nolan et al. (2007)'s modeling study found that intensification was more efficient when the convective heating was located inside the RMW. Given our and DeMaria et al. (2012)'s results of higher inner core flash densities in nonintensifying TCs, this would imply most inner core lightning is occurring outside the RMW. The authors are currently investigating this hypothesis and will present the results in a future study.

The opposite relationship was found in the outer rainband region, where higher flash densities tended to occur in intensifying TCs (Fig. 13). The TDTS group in the ENP had a normalized flash density in intensifying TCs that was more than double the normalized flash density in nonintensifying TCs; this result is statistically significant at the 95% confidence level. Weak ENP hurricanes (H1H2) also had a higher flash density in intensifying TCs, and major hurricanes (H3H5) had the reverse relationship of higher flash densities in nonintensifying TCs, though both of these results exhibited low confidence in the bootstrap resampling method. The NA TDTS strength storms had very similar normalized flash densities in intensifying and nonintensifying TCs; the difference between the two was small and not statistically significant. Weak NA hurricanes had higher outer rainband flash densities in nonintensifying storms; however, strong NA hurricanes had a statistically significant higher flash density in intensifying TCs. DeMaria et al. (2012) found the

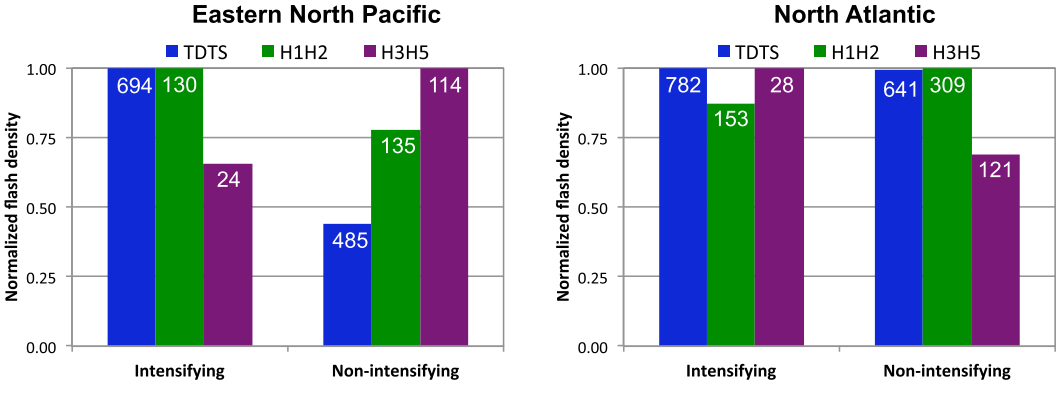

FIG. 13. As in Fig. 12, but for the outer rainbands (100–300 km).

same relationship, with higher flash densities in the outer rainbands of intensifying TCs, in their adjusted WWLLN dataset.

It is unclear why stronger convection in the outer rainbands would favor intensification. DeMaria et al. (2012) hypothesized that rainband lightning is a measure of the convective instability in the storm environment. However, Wang (2009) describes several reasons why convection in the outer rainbands has a *negative* impact on TC intensity: convection in the outer rainbands can 1) reduce the amount of mass converged in the eyewall, 2) cause compensating subsidence over the eyewall convection, 3) flux low equivalent potential temperature air into the boundary layer inflow, and 4) hydrostatically reduce the radial pressure gradient. All of these impacts would favor TC weakening, not intensification; thus, more research is necessary to understand the association between outer rainband lightning and TC intensity change. Observational analysis of how the outer rainbands communicate with the inner core and TC intensity is suggested for future work.

4. Summary and conclusions

While several studies have utilized global lightning network data (such as the WWLLN) to investigate lightning in TCs, most of them have been focused on the northwest Pacific or NA basins. This study's primary focus is on lightning flashes, detected by WWLLN, in ENP TCs, with the NA used for comparison. Although the ENP has been widely ignored, studies by DeMaria et al. (2012) and Leary and Ritchie (2009) have provided some preliminary insight into ENP lightning activity in TCs. The relationship of lightning activity to SST, the diurnal cycle, storm motion and vertical wind shear, and intensity changes are examined in the present study. The main findings are summarized below:

- More lightning flashes occur over warmer SSTs, with the highest flash rates occurring when SSTs are between 28° and 30°C in both the ENP and NA.
- The diurnal cycle in ENP TCs is characterized by increased activity between 1700 and 0900 LST, with an overall peak at 0800 LST. The diurnal cycle in NA TCs is characterized by a primary peak in the early morning hours (0100 LST) and a secondary peak in the late morning (0900–1100 LST). Both basins have minimal lightning activity within 300 km of the TC center in the afternoon hours.
- The radial distribution of flash counts has two maxima, similar to previous studies: one located in the region of the eyewall and one in the outer rainbands. The eyewall maximum moves radially inward with increasing TC strength, likely due to eyewall contraction, while the outer rainband maximum remains around 290 km.
- Vertical wind shear dominates storm motion in controlling the overall azimuthal pattern of convection in both basins, confirming the results of CM03. The ENP and NA had motion asymmetries that were 90°–180° out of phase with each other, which reflects the shear and motion vector differences between the two basins. Both basins exhibited the expected downshear left maximum in the inner core and downshear right maximum in the outer rainbands. The ENP lightning was found to be influenced by the motion for faster motion ITPs when the shear and motion vectors opposed each other; this asymmetry did not appear in the NA.
- The lightning flash densities in intensifying and nonintensifying TCs were similar to the results of DeMaria et al. (2012)'s study, although we did not apply adjustment factors to the WWLLN data as they did. Higher normalized flash densities were typically observed in the inner core of nonintensifying TCs, with statistical significance in ENP TDTS/H1H2 and NA H1H2. Higher flash densities in the outer rainbands tended to occur in intensifying TCs, with statistical significance in ENP TDTS and NA H3H5.

The characteristics described in this study provide a baseline for future studies examining TC lightning activity in the ENP. An understanding of why the ENP is more sensitive to convective motion asymmetries than the NA is needed. It was briefly mentioned that a radially outward propagating feature in the lightning field was observed in sync with the diurnal cycle mentioned in Dunion et al. (2014); more research is needed to understand the importance of this feature and its sporadic occurrence. The association between lightning activity and intensity change is a topic that needs much more attention as well, since a full understanding of the associative relationship has the potential to improve TC intensity forecasts, especially in regions like the ENP that are not frequently sampled by aircraft. The launch of the GOES-R satellite and its GLM instrument in 2016 will provide unprecedented, continuous total lightning observations over ENP and NA TCs; the results of this study, along with other oceanic TC lightning studies, will lay the foundation for interpreting and utilizing the GLM data in TC observations and forecasts.

Acknowledgments. The authors thank four anonymous reviewers for their helpful comments that

improved the quality of this manuscript. The authors would also like to thank Fernando Oropeza and Graciela Raga from the Universidad Nacional Autónoma de México for their involvement in this research project, which began at the University of California, Los Angeles (UCLA), with support from the University of California Institute for Mexico and the United States (UC MEXUS) and Consejo Nacional de Ciencia y Tecnología (CONACYT) Grant CN-10-431. The authors wish to thank the World Wide Lightning Location Network (http://wwlln.net), a collaboration among over 50 universities and institutions, for providing the lightning location data used in this paper. This work was completed with NASA Award NNX12AJ81G.

REFERENCES

Abarca, S. F., K. L. Corbosiero, and T. J. Galarneau Jr., 2010: An evaluation of the Worldwide Lightning Location Network (WWLLN) using the National Lightning Detection Network (NLDN) as ground truth. *J. Geophys. Res.*, **115**, D18206, doi:10.1029/2009JD013411.

——, ——, and D. Vollaro, 2011: The World Wide Lightning Location Network and convective activity in tropical cyclones. *Mon. Wea. Rev.*, **139**, 175–191, doi:10.1175/2010MWR3383.1.

Boccippio, D. J., and Coauthors, 2000: The Optical Transient Detector (OTD): Instrument characteristics and cross-sensor validation. *J. Atmos. Oceanic Technol.*, **17**, 441–458, doi:10.1175/1520-0426(2000)017<0441:TOTDOI>2.0.CO;2.

——, W. J. Koshak, and R. J. Blakeslee, 2002: Performance assessment of the Optical Transient Detector and Lightning Imaging Sensor. Part I: Predicted diurnal variability. *J. Atmos. Oceanic Technol.*, **19**, 1318–1332, doi:10.1175/1520-0426(2002)019<1318:PAOTOT>2.0.CO;2.

Bowman, K. P., and M. D. Fowler, 2015: The diurnal cycle of precipitation in tropical cyclones. *J. Climate*, **28**, 5325–5334, doi:10.1175/JCLI-D-14-00804.1.

Camargo, S. J., A. W. Robertson, A. G. Barnston, and M. Ghil, 2008: Clustering of eastern North Pacific tropical cyclone tracks: ENSO and MJO effects. *Geochem. Geophys. Geosyst.*, **9**, Q06V05, doi:10.1029/2007GC001861.

Cecil, D. J., and E. J. Zipser, 1999: Relationship between tropical cyclone intensity and satellite-based indicators of inner core convection: 85-GHz ice-scattering signature and lightning. *Mon. Wea. Rev.*, **127**, 103–123, doi:10.1175/1520-0493(1999)127<0103:RBTCIA>2.0.CO;2.

——, D. E. Buechler, and R. J. Blakeslee, 2014: Gridded lightning climatology from TRMM-LIS and OTD: Dataset description. *Atmos. Res.*, **135–136**, 404–414, doi:10.1016/j.atmosres.2012.06.028.

Chen, S. S., J. A. Knaff, and F. D. Marks Jr., 2006: Effects of vertical wind shear and storm motion on tropical cyclone rainfall asymmetries deduced from TRMM. *Mon. Wea. Rev.*, **134**, 3190–3208, doi:10.1175/MWR3245.1.

Corbosiero, K. L., and J. Molinari, 2002: The effects of vertical wind shear on the distribution of convection in tropical cyclones. *Mon. Wea. Rev.*, **130**, 2110–2123, doi:10.1175/1520-0493(2002)130<2110:TEOVWS>2.0.CO;2.

——, and ——, 2003: The relationship between storm motion, vertical wind shear, and convective asymmetries in tropical cyclones. *J. Atmos. Sci.*, **60**, 366–376, doi:10.1175/1520-0469(2003)060<0366:TRBSMV>2.0.CO;2.

——, M. J. Dickinson, and L. F. Bosart, 2009: The contribution of eastern North Pacific tropical cyclones to the rainfall climatology of the southwest United States. *Mon. Wea. Rev.*, **137**, 2415–2435, doi:10.1175/2009MWR2768.1.

Cummins, K. L., and M. J. Murphy, 2009: An overview of lightning locating systems: History, techniques, and data uses, with an in depth look at the U.S. NLDN. *IEEE Trans. Electromag. Compat.*, **51**, 499–518, doi:10.1109/TEMC.2009.2023450.

——, ——, E. A. Bardo, W. L. Hiscox, R. B. Pyle, and A. E. Pifer, 1998: A combined TOA/MDF technology upgrade of the U.S. National Lightning Detection Network. *J. Geophys. Res.*, **103**, 9035–9044, doi:10.1029/98JD00153.

——, R. B. Pyle, and G. Fournier, 1999: An integrated North American lightning detection network. Preprints, *11th Int. Conf. on Atmospheric Electricity*, Guntersville, AL, Amer. Meteor. Soc., 218–221.

DeMaria, M., and J. Kaplan, 1994: A Statistical Hurricane Intensity Prediction Scheme (SHIPS) for the Atlantic basin. *Wea. Forecasting*, **9**, 209–220, doi:10.1175/1520-0434(1994)009<0209:ASHIPS>2.0.CO;2.

——, R. T. DeMaria, J. A. Knaff, and D. Molenar, 2012: Tropical cyclone lightning and rapid intensity change. *Mon. Wea. Rev.*, **140**, 1828–1842, doi:10.1175/MWR-D-11-00236.1.

Dunion, J. P., C. D. Thorncroft, and C. S. Velden, 2014: The tropical cyclone diurnal cycle of mature hurricanes. *Mon. Wea. Rev.*, **142**, 3900–3919, doi:10.1175/MWR-D-13-00191.1.

Farfán, L. M., E. J. Alfaro, and T. Cavazos, 2013: Characteristics of tropical cyclones making landfall on the Pacific coast of Mexico: 1970–2010. *Atmósfera*, **26**, 163–182, doi:10.1016/S0187-6236(13)71070-1.

Frank, W. M., 1977: The structure and energetics of the tropical cyclone. I. Storm structure. *Mon. Wea. Rev.*, **105**, 1119–1135, doi:10.1175/1520-0493(1977)105<1119:TSAEOT>2.0.CO;2.

Fu, R., A. D. Del Genio, and W. B. Rossow, 1994: Influence of ocean surface conditions on atmospheric vertical thermodynamic structure and deep convection. *J. Climate*, **7**, 1092–1108, doi:10.1175/1520-0442(1994)007<1092:IOOSCO>2.0.CO;2.

Gao, S., and X. Li, 2008: Diurnal variations in tropical oceanic convection. *Cloud-Resolving Modeling of Convective Processes*, Springer-Dordrecht, 121–136.

Goodman, S. J., and Coauthors, 2013: The GOES-R Geostationary Lightning Mapper (GLM). *Atmos. Res.*, **125–126**, 34–49, doi:10.1016/j.atmosres.2013.01.006.

Gray, W. M., 1968: Global view of the origin of tropical disturbances and storms. *Mon. Wea. Rev.*, **96**, 669–700, doi:10.1175/1520-0493(1968)096<0669:GVOTOO>2.0.CO;2.

——, and R. W. Jacobson Jr., 1977: Diurnal variation of deep cumulus convection. *Mon. Wea. Rev.*, **105**, 1171–1188, doi:10.1175/1520-0493(1977)105<1171:DVODCC>2.0.CO;2.

Holle, R. L., and M. J. Murphy, 2015: Lightning in the North American monsoon: An exploratory climatology. *Mon. Wea. Rev.*, **143**, 1970–1977, doi:10.1175/MWR-D-14-00363.1.

Hutchins, M. L., R. H. Holzworth, K. S. Virts, J. M. Wallace, and S. Heckman, 2013: Radiated VLF energy differences of land and oceanic lightning. *Geophys. Res. Lett.*, **40**, 2390–2394, doi:10.1002/grl.50406.

Janowiak, J. E., P. A. Arkin, and M. Morrissey, 1994: An examination of the diurnal cycle in oceanic tropical rainfall using satellite and in situ data. *Mon. Wea. Rev.*, **122**, 2296–2311, doi:10.1175/1520-0493(1994)122<2296:AEOTDC>2.0.CO;2.

Jones, S. C., 1995: The evolution of vorticies in vertical shear. I: Initially barotropic vortices. *Quart. J. Roy. Meteor. Soc.*, **121**, 821–851, doi:10.1002/qj.49712152406.

Knaff, J. A., S. P. Longmore, and D. A. Molenar, 2014: An objective satellite-based tropical cyclone size climatology. *J. Climate*, **27**, 455–476, doi:10.1175/JCLI-D-13-00096.1.

Kossin, J. P., 2002: Daily hurricane variability inferred from GOES infrared imagery. *Mon. Wea. Rev.*, **130**, 2260–2270, doi:10.1175/1520-0493(2002)130<2260:DHVIFG>2.0.CO;2.

Kucienska, B., G. B. Raga, and V. M. Torres-Puente, 2012: Climatology of precipitation and lightning over the Pacific coast of southern Mexico retrieved from Tropical Rainfall Measuring Mission satellite products and World Wide Lightning Location Network data. *Int. J. Remote Sens.*, **33**, 2831–2850, doi:10.1080/01431161.2011.621905.

Landsea, C. W., and J. L. Franklin, 2013: Atlantic hurricane database uncertainty and presentation of a new database format. *Mon. Wea. Rev.*, **141**, 3576–3592, doi:10.1175/MWR-D-12-00254.1.

Lau, K.-M., H.-T. Wu, and S. Bony, 1997: The role of large-scale atmospheric circulation in the relationship between tropical convection and sea surface temperature. *J. Climate*, **10**, 381–392, doi:10.1175/1520-0442(1997)010<0381:TROLSA>2.0.CO;2.

Lay, E. H., R. H. Holzworth, C. J. Rodger, J. N. Thomas, O. Pinto Jr., and R. L. Dowden, 2004: WWLL global lightning detection system: Regional validation study in Brazil. *Geophys. Res. Lett.*, **31**, L03102, doi:10.1029/2003GL018882.

——, A. R. Jacobson, R. H. Holzworth, C. J. Rodger, and R. L. Dowden, 2007: Local time variation in land/ocean lightning flash density as measured by the World Wide Lightning Location Network. *J. Geophys. Res.*, **112**, D13111, doi:10.1029/2006JD007944.

Leary, L. A., and E. A. Ritchie, 2009: Lightning flash rates as an indicator of tropical cyclone genesis in the eastern North Pacific. *Mon. Wea. Rev.*, **137**, 3456–3470, doi:10.1175/2009MWR2822.1.

Molinari, J., P. Moore, and V. Idone, 1999: Convective structure of hurricanes as revealed by lightning locations. *Mon. Wea. Rev.*, **127**, 520–534, doi:10.1175/1520-0493(1999)127<0520:CSOHAR>2.0.CO;2.

——, D. Vollaro, S. Skubis, and M. Dickinson, 2000: Origins and mechanisms of eastern Pacific tropical cyclogenesis: A case study. *Mon. Wea. Rev.*, **128**, 125–139, doi:10.1175/1520-0493(2000)128<0125:OAMOEP>2.0.CO;2.

Nesbitt, S. W., and E. J. Zipser, 2003: The diurnal cycle of rainfall and convective intensity according to three years of TRMM measurements. *J. Climate*, **16**, 1456–1475, doi:10.1175/1520-0442-16.10.1456.

Nolan, D., Y. Moon, and D. P. Stern, 2007: Tropical cyclone intensification from asymmetric convection: Energetics and efficiency. *J. Atmos. Sci.*, **64**, 3377–3405, doi:10.1175/JAS3988.1.

Pan, L., X. Qie, D. Liu, D. Wang, and J. Yang, 2010: The lightning activities in super typhoons over the Northwest Pacific. *Sci. China Earth Sci.*, **53**, 1241–1248, doi:10.1007/s11430-010-3034-z.

——, ——, and D. Wang, 2014: Lightning activity and its relation to the intensity of typhoons over the Northwest Pacific Ocean. *Adv. Atmos. Sci.*, **31**, 581–592, doi:10.1007/s00376-013-3115-y.

Price, C., M. Asfur, and Y. Yair, 2009: Maximum hurricane intensity preceded by increase in lightning frequency. *Nat. Geosci.*, **2**, 329–332, doi:10.1038/ngeo477.

Reasor, P. D., M. T. Montgomery, and L. D. Grasso, 2004: A new look at the problem of tropical cyclones in vertical shear flow: Vortex resiliency. *J. Atmos. Sci.*, **61**, 3–22, doi:10.1175/1520-0469(2004)061<0003:ANLATP>2.0.CO;2.

Reynolds, R. W., and D. C. Marsico, 1993: An improved real-time global sea surface temperature analysis. *J. Climate*, **6**, 114–119, doi:10.1175/1520-0442(1993)006<0114:AIRTGS>2.0.CO;2.

Rodger, C. J., S. Werner, J. B. Brundell, E. H. Lay, N. R. Thomson, R. H. Holzworth, and R. L. Dowden, 2006: Detection efficiency of the VLF World-Wide Lightning Location Network (WWLLN): Initial case study. *Ann. Geophys.*, **24**, 3197–3214, doi:10.5194/angeo-24-3197-2006.

Rogers, R., P. Reasor, and S. Lorsolo, 2013: Airborne Doppler observations of the inner-core structural differences between intensifying and steady-state tropical cyclones. *Mon. Wea. Rev.*, **141**, 2970–2991, doi:10.1175/MWR-D-12-00357.1.

Romps, D. M., J. T. Seeley, D. Vollaro, and J. Molinari, 2014: Projected increase in lightning strikes in the United States due to global warming. *Science*, **346**, 851–853, doi:10.1126/science.1259100.

Rudlosky, S. D., and D. T. Shea, 2013: Evaluation WWLLN performance relative to TRMM/LIS. *Geophys. Res. Lett.*, **40**, 2344–2348, doi:10.1002/grl.50428.

Shapiro, L. J., 1983: The asymmetric boundary layer flower under a translating hurricane. *J. Atmos. Sci.*, **40**, 1984–1998, doi:10.1175/1520-0469(1983)040<1984:TABLFU>2.0.CO;2.

——, and H. E. Willoughby, 1982: The response of balanced hurricanes to local sources of heat and momentum. *J. Atmos. Sci.*, **39**, 378–394, doi:10.1175/1520-0469(1982)039<0378:TROBHT>2.0.CO;2.

Stevenson, S. N., K. L. Corbosiero, and J. Molinari, 2014: The convective evolution and rapid intensification of Hurricane Earl (2010). *Mon. Wea. Rev.*, **142**, 4364–4380, doi:10.1175/MWR-D-14-00078.1.

Thomas, J. N., N. N. Solorzano, S. A. Cummer, and R. H. Holzworth, 2010: Polarity and energetics of inner core lightning in three intense North Atlantic hurricanes. *J. Geophys. Res.*, **115**, A00E15, doi:10.1029/2009JA014777.

Thomsen, G. L., R. K. Smith, and M. T. Montgomery, 2015: Tropical cyclone flow asymmetries induced by a uniform flow revisited. *J. Adv. Model. Earth Syst.*, **7**, 1265–1284, doi:10.1002/2015MS000477.

Trenberth, K., 2005: Uncertainty in hurricanes and global warming. *Science*, **308**, 1753–1754, doi:10.1126/science.1112551.

Vigh, J. L., and W. H. Schubert, 2009: Rapid development of the tropical cyclone warm core. *J. Atmos. Sci.*, **66**, 3335–3350, doi:10.1175/2009JAS3092.1.

Virts, K. S., J. M. Wallace, M. L. Hutchins, and R. Holzworth, 2013: Highlights of a new ground-based, hourly global lightning climatology. *Bull. Amer. Meteor. Soc.*, **94**, 1381–1391, doi:10.1175/BAMS-D-12-00082.1.

——, ——, ——, and R. H. Holzworth, 2015: Diurnal and seasonal lightning variability over the Gulf Stream and Gulf of Mexico. *J. Atmos. Sci.*, **72**, 2657–2665, doi:10.1175/JAS-D-14-0233.1.

Waliser, D. E., and N. E. Graham, 1993: Convective cloud systems and warm-pool sea surface temperatures: Coupled interactions and self-regulation. *J. Geophys. Res.*, **98**, 12 881–12 893, doi:10.1029/93JD00872.

Wang, Y., 2009: How do outer spiral rainbands affect tropical cyclone structure and intensity? *J. Atmos. Sci.*, **66**, 1250–1273, doi:10.1175/2008JAS2737.1.

Watt, A. D., 1967: *VLF Radio Engineering.* Pergamon Press, 703 pp.

Willoughby, H. E., 1990: Temporal changes of the primary circulation in tropical cyclones. *J. Atmos. Sci.*, **47**, 242–264, doi:10.1175/1520-0469(1990)047<0242:TCOTPC>2.0.CO;2.

Zhang, W., Y. Zhang, D. Zheng, F. Wang, and L. Xu, 2015: Relationship between lightning activity and tropical cyclone intensity over the northwest Pacific. *J. Geophys. Res. Atmos.*, **120**, 4072–4089, doi:10.1002/2014JD022334.

Corrigendum

STEPHANIE N. STEVENSON AND KRISTEN L. CORBOSIERO

University at Albany, State University of New York, Albany, New York

SERGIO F. ABARCA

Environmental Modeling Center, I. M. Systems Group, and NOAA/NWS/NCEP, College Park, Maryland

(Manuscript received 22 July 2016, in final form 26 September 2016)

An error was discovered in the direction of the deep-layer vertical wind shear vector obtained from the Statistical Hurricane Intensity Prediction Scheme (SHIPS) database in Stevenson et al. (2016). In the original submission, postprocessed files were used for 2005–13, and real-time text files were used for 2014 because the postprocessed files were not available for 2014 prior to submission. The authors were unaware of the differences in shear direction between the two datasets: the postprocessed files use the shear heading (i.e., the direction the shear is going *toward*), while the real-time text files use the direction the shear is *coming from* (M. DeMaria 2016, personal communication). Thus, the shear directions used for tropical cyclones (TCs) in 2014 were off by 180°. This impacted 359 (18%) individual time periods (ITPs) in the eastern North Pacific and 143 (6%) ITPs in the North Atlantic. Figures 8, 10, and 11 have changed as a result of this error.

While small changes are evident in icosagon magnitudes in Fig. 8, the interpretation of the figure remains the same. Lightning peaks downshear left in the inner core and downshear right in the outer rainbands, with the relationship becoming stronger as the shear magnitude increases.

Slight changes are also evident in the histogram of the angle between the shear and motion vectors shown in Fig. 10. The general patterns discussed between the eastern North Pacific and the North Atlantic remain the same despite these changes.

The largest differences occur in Fig. 11. Stevenson et al. (2016) discussed the peak of lightning occurring downmotion rather than downshear for eastern North Pacific cases where the motion and shear vectors opposed one another (i.e., are approximately 180° apart). This signal becomes less evident with the corrected shear directions for 2014. The overall maximum shifted toward the expected downshear-left position in the inner core and downshear-right position in the outer rainbands. However, there is still an indication that motion plays a larger role in the eastern North Pacific than it does in the North Atlantic in this opposite shear and motion scenario, particularly for fast-moving TCs (not shown). This difference between the basins remains a topic for future research.

REFERENCE

Stevenson, S. N., K. L. Corbosiero, and S. F. Abarca, 2016: Lightning in eastern North Pacific tropical cyclones: A comparison to the North Atlantic. *Mon. Wea. Rev.*, **144**, 225–239, doi:10.1175/MWR-D-15-0276.1.

Corresponding author address: Stephanie N. Stevenson, Department of Atmospheric and Environmental Sciences, University at Albany, State University of New York, 1400 Washington Ave., Albany, NY 12222.
E-mail: sstevenson@albany.edu

DOI: 10.1175/MWR-D-16-0283.1

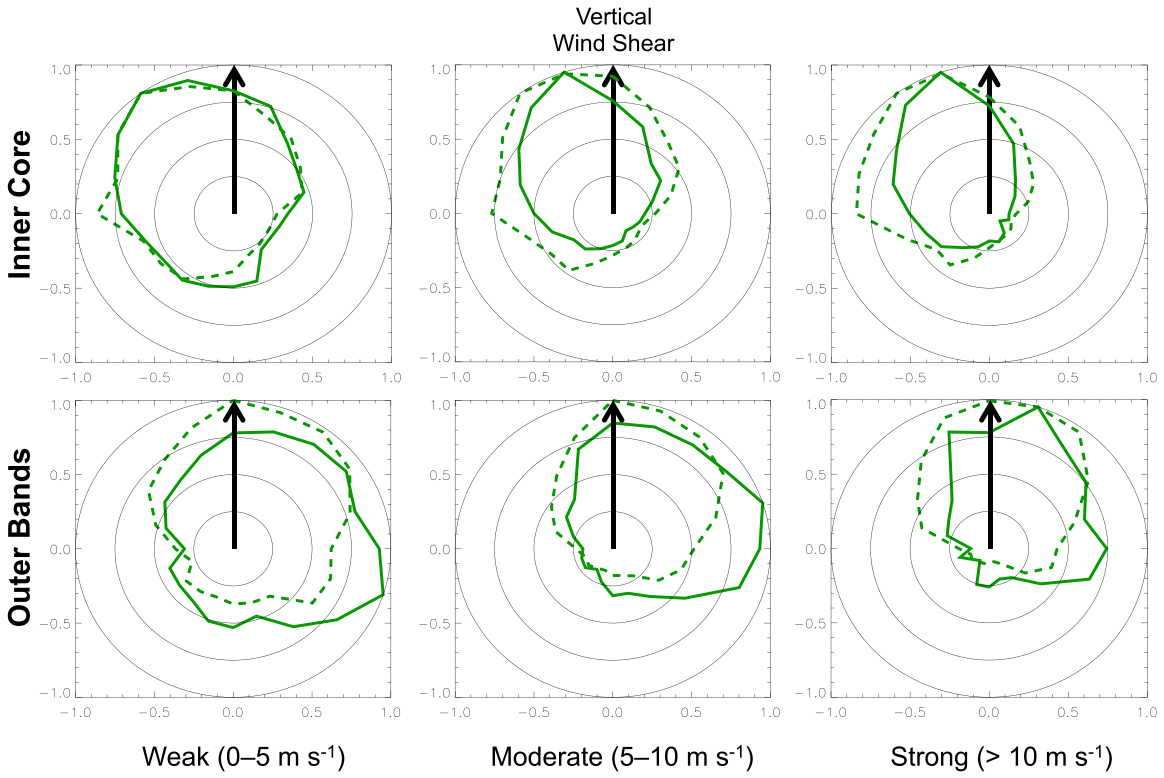

FIG. 8. Icosagons indicating the most common locations of lightning flashes in the (top) inner core and (bottom) outer rainbands with respect to the shear vector (black arrow) for eastern North Pacific (solid) and North Atlantic (dashed) TCs. The icosagons are displayed for various shear values: (left) weak (0–5 m s^{-1}), (middle) moderate (5–10 m s^{-1}), and (right) strong (>10 m s^{-1}).

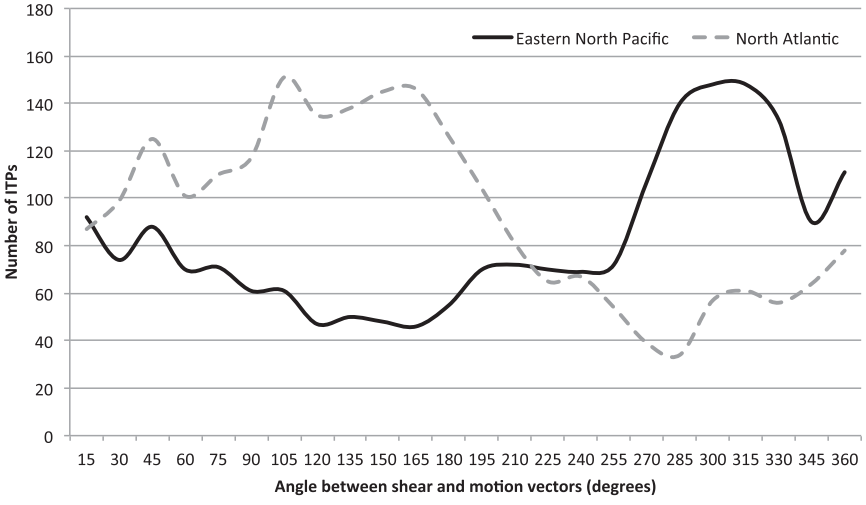

FIG. 10. Histogram of the number of 6-hourly individual time periods (ITPs) corresponding to various angles between the shear and motion vectors for eastern North Pacific (solid black) and North Atlantic (dashed gray) TCs. The angle is measured counterclockwise from the shear vector to the motion vector.

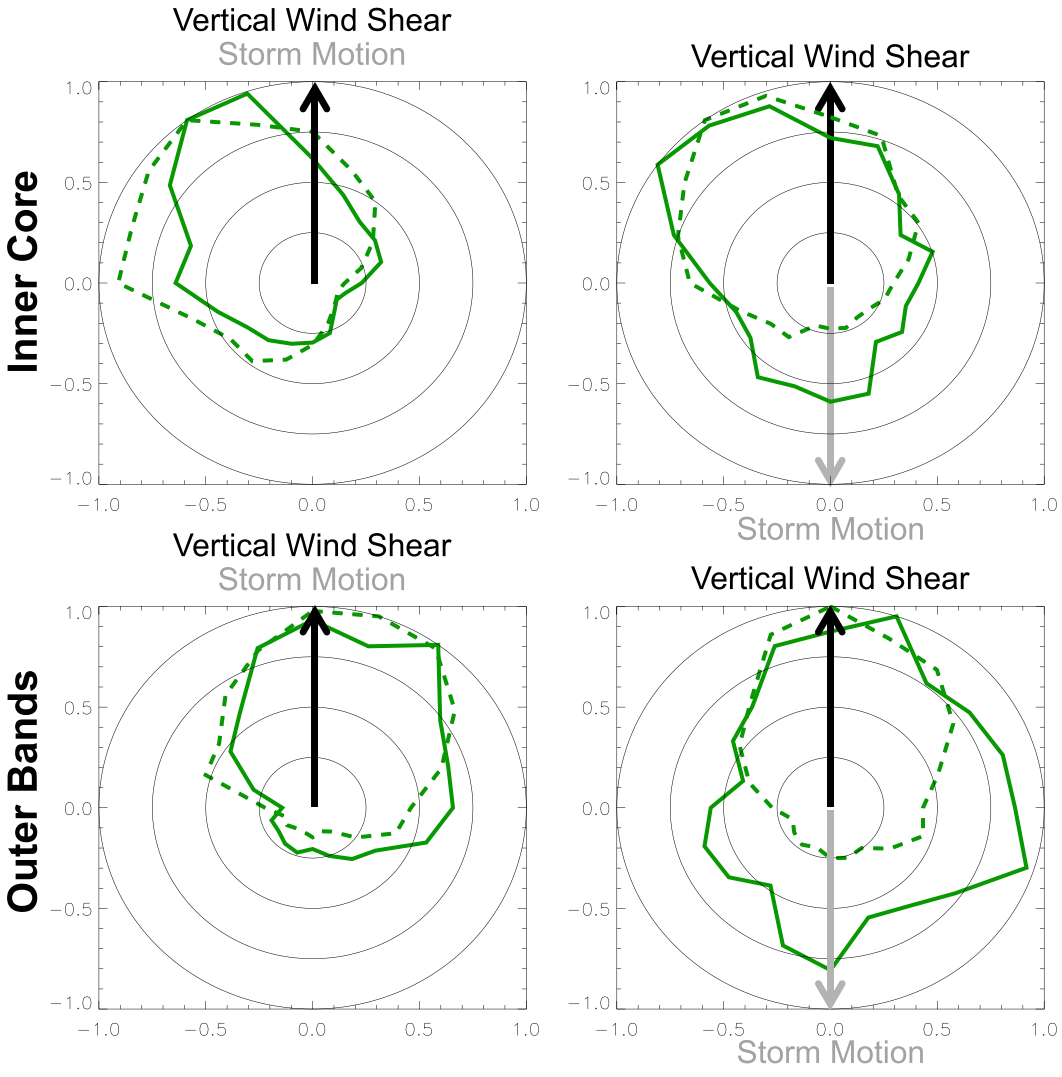

FIG. 11. Icosagons indicating the most common locations of lightning flashes in the (top) inner core and (bottom) outer rainbands with respect to the shear (black arrow) and motion (gray arrow) vector for the eastern North Pacific (solid) and North Atlantic (dashed). (left) ITPs where the shear and motion vector are aligned (>37.5° and <22.5°), and (right) ITPs where the shear and motion vector are opposed (157.5°–202.5°). All motion speeds and shear magnitudes are included.